Article

Switchable Enantioselective Three- and Four-Dimensional Dynamic Gas Chromatography-Mass Spectrometry: Example Study of On-column Molecular Interconversion

Yong Foo Wong, Chadin Kulsing, and Philip John Marriott

Anal. Chem., **Just Accepted Manuscript** • DOI: 10.1021/acs.analchem.7b00853 • Publication Date (Web): 11 Apr 2017

Switchable Enantioselective Three- and Four-Dimensional Dynamic Gas Chromatography-Mass Spectrometry: Example Study of On-column Molecular Interconversion

Yong Foo Wong, Chadin Kulsing and Philip J. Marriott*

Australian Centre for Research on Separation Science, School of Chemistry, Monash University, Wellington Road, Clayton, VIC 3800, Australia.

ABSTRACT: A novel hybrid on-line enantioselective four-dimensional dynamic GC (*e*4D-*D*GC) approach to study reversible molecular interconversion through specific isolation of a diastereo, and enantiopure oxime, 2-phenylpropanaldehyde oxime from prior multidimensional separation, is described. It incorporates a pre-enantioseparation step that applies comprehensive two-dimensional GC (GC×GC), prior to multiple microfluidic (Deans) switching for selection of components of a diastereomeric (*E*,*Z*) and enantiomeric (*R*,*S*) oxime into a third reactor column where isomerization occurs. This is followed by *E*/*Z* separation in a fourth analytical column. The enantioselective first dimension ($^1D_{enant}$) yields enantioseparation of *E*(*R*), *Z*(*R*), *E*(*S*) and *Z*(*S*) isomers, with a characteristic interconversion zone between the *E* and *Z* isomers. However these are contaminated with underlying stereoisomers. Selected separation regions were then modulated and separated using a second dimension (^2D) column via GC×GC, resolving the interfering stereoisomers. Individual pure enantiomers were then selectively heart-cut from within the 2D separation space, cryofocussed, then eluted on a ^3D reactor column for $E \rightleftharpoons Z$ isomerization under controlled oven temperature and flow. Heart-cuts taken over the resulting interconversion distribution were cryotrapped at the inlet of a ^4D column, on which achiral separation allows precise quantification of each *E* and *Z* isomer of the enantiomer. From peak areas and isomerization time, the forward and backward rate constants ($k_{E\rightarrow Z}$ and $k_{Z\rightarrow E}$) were determined. The described methodology is suited to other configurationally labile molecules (for instance, hydrazones and imines) which exhibit isomerization, and can be used to isolate individual compounds from multicomponent samples, without requiring pure compound synthesis, or complex mathematical models or in-silico simulations.

Investigation of the molecular dynamics of configurationally labile stereoisomers has become increasingly important across a broad range of research areas (e.g. drug development,[1] protein folding,[2] biochemistry,[3] supramolecular chemistry,[4] etc.). Transformation or interconversion processes of labile isomers can be treated as a change toward racemic or non-racemic mixtures of stereoisomers at thermodynamic equilibrium. Two different processes can be identified, (i) irreversible structural transformation (e.g. and decomposition[5]), and (ii) reversible molecular interconversion (e.g. racemization[6], enantiomerization[7] and diastereomerization[4]). Dynamic chromatography has been used for the study of reversible configurational changes, including gas chromatography (GC),[8-10] high performance liquid chromatography,[1,2,11-13] capillary electrophoresis,[14-16] thin layer chromatography,[17] supercritical fluid chromatography,[18,19] and in conjunction with nuclear magnetic resonance.[20] Interconversion, phase partitioning, and distribution of the *E* and *Z* isomers of oximes in a 'reactor column' can be represented by Supporting Information **Figure S1**.

For 'dynamic reaction' in single dimensional (1D) chromatography, non-Gaussian elution profiles may be observed, indicating on-column interconversion or decomposition during separation. The shapes of the peaks (peak-broadening; plateau-formation between two terminal peaks; peak coalescence) depend on the stereochemical stability or lability of the investigated molecules, and the rate of 'reaction' of the isomers under prevailing conditions on the chromatographic separation timescale. Chromatographically, distorted distributions of isomers constituting interconversion profiles confounds direct estimation of epimeric, isomeric or enantiomeric ratios at any given point. This normally requires iterative comparison of experimental and simulated elution profiles to assess interconversion rate constants and Gibbs activation. The Schurig group investigated many such molecular processes of chiral molecules using dynamic chromatographic approaches.[9,11,14,15,21,22]

In *D*GC experiments, an interconversion or plateau region will arise from original injected peaks if the prevailing thermal energy does not greatly exceed the interconversion barrier energy, otherwise 'peak coalescence of the third-type' may arise.[23] Determination of kinetic and activation data for interconversion is based on the total envelope shape of the dynamic chromatogram, accompanied by mathematical modelling or simulation. Trapp and Schurig developed a Windows-based computer program (ChromWin and ChromWin 2D) for interpretation of the interconversion process based on simulation, employing the theoretical plate model, stochastic model, and a modified stochastic model to describe chromatographic elution.[9,24,25] Krupčik et al. developed computer assisted methods to deconvolute interconversion profiles.[8,26] In 2006, Trapp developed a unified equation to calculate rate constants of a first-order reaction directly from chromatographic parameters (peak width; retention time), applying it to calculate kinetic data for alkylated diaziridines.[27,28] The program DCXplorer was further introduced by Trapp, utilizing the unified equation of chromatography for evaluation of interconversion barriers.[29,30]

Multidimensional GC techniques (e.g. stopped-flow MDGC and comprehensive two-dimensional GC; GC×GC), have been introduced to physically deconvolute isomeric forms underneath the interconversion plateau. Trapp and Schurig developed stopped-flow MDGC for the determination of epimerization barriers of stereolabile compounds (e.g. Tröger's base, chalcogran, etc.), with $\Delta G^{\#}_{gas}$ values ranging from 70 kJ mol^{-1} to 200 kJ mol^{-1}.[9,10,31] Marriott and co-workers applied high resolution GC×GC to study oxime interconversions, with novel presentation of the isomerization process over the 2D chromatographic space where the second dimension (^{2}D) resolves *E* and *Z* isomers across the distribution.[25,32-34] Recently, Kröger et al. employed enantioselective columns in both ^{1}D and ^{2}D to investigate reversible molecular interconversion behavior of a chiral aromatic oxime, illustrating features of molecular reversible process in the 2D patterns.[34]

The present work demonstrates a novel enantioselective four-dimensional *D*GC (*e*4D-*D*GC) system with accurate mass time-of-flight mass spectrometry (accTOFMS) for the microscopic study of molecular interconversion of a chiral aromatic oxime. It operates as a sequential enantioselective GC×GC-MDGC-GC system, to allow unique isolation of the modulated peaks of diastereo- and enantiopure isomers in 2D space (i.e. by heart-cutting (H/C) as described by Mitrevski and Marriott[35]), prior to study of the dynamic behavior of each individual compound. Here we report details of performance, reliability and applicability of *e*4D-*D*GC–accTOFMS for direct determination of isomeric ratios and rate constants of reversible interconversion of 2-phenylpropanaldehyde oxime. Data are used to discuss reversible molecular processes of the interconverting molecules on the time-scale of chromatographic elution.

EXPERIMENTAL SECTION

Reagents and chemicals. 2-phenylpropanaldehyde (≥ 97%), and 1-tridecanol (≥ 97%) were purchased from Sigma-Aldrich (St. Louis, MO). HPLC grade *n*-hexane and dichloromethane were purchased from Merck (Darmstadt, Germany).

4D analysis: GC$_{enant}$×GC$_{IL}$-*D*GC-GC$_{np}$–accTOFMS. Enantioselective dynamic multidimensional experiments were conducted on an Agilent 7890A GC coupled to an Agilent 7200 accurate mass QTOFMS (Agilent Technologies, Mulgrave, Australia), equipped with a flame ionization detector (FID) and PAL3 Auto Sampler (CTC Analytics AG, Zwingen, Switzerland), retrofitted with an Everest model longitudinally modulated cryogenic system (LMCS; Chromatography Concepts, Doncaster, Australia). The GC×GC experiments were performed using a MEGA-DEX DET-Beta column as ^{1}D$_{enant}$ (diethyl tertbutylsilyl-β-cyclodextrin; 25 m × 0.25 mm × 0.25 µm d_f; MEGA s.n.c, Milan, Italy), and a SLB-IL111 column (1.8 m × 0.1 mm × 0.1 µm d_f; Supelco, Bellefonte, PA) as ^{2}D column (^{2}D$_{IL}$). A deactivated Press-Tight connector (Restek Corp, Bellefonte, PA) was used to connect the two columns. SUPELCOWAX® 10 column (15 m × 0.25 mm × 0.25 µm d_f) was used as ^{3}D reactor column (^{3}D$_{react}$), and a DB-5ms Ultra Inert column (30 m × 0.25 mm × 0.25 µm d_f; Agilent) as fourth dimension column (^{4}D$_{np}$). A microfluidic Deans switch (DS; Agilent) for heart-cut (H/C) effluent switching was used to interface the end of ^{2}D$_{IL}$ to the start of ^{3}D$_{react}$ with a deactivated fused-silica tubing (DFS; 1.8 m × 0.1 mm I.D.) as transfer line to the FID. H/C switching of effluent flow from ^{1}D$_{enant}$ to either ^{3}D$_{react}$ or the FID was controlled through the events option in MassHunter software via a three channel auxiliary electronic pressure control (EPC) module (G1570A; Agilent). The modulator was held at a constant modulation temperature (T_M) of 20 °C and modulation period (P_M) of 8 s, with carbon dioxide as cryogen coolant. FID (250 ˚C) was operated at a sampling frequency of 100 Hz to monitor the very narrow GC peaks eluting from ^{2}D$_{IL}$. A schematic of the system used here is shown in **Figure 1A**, for GC×GC mode (without heart-cutting, indicated by orange arrow) and for transfer of heart-cuts to the ^{3}D$_{react}$ column (indicated by red arrow), respectively. A workflow describing the different steps in the operation is shown in **Figure 1B**.

An SGE liquid CO_2 cryogenic trapping device (CT; Trajan Scientific, Ringwood, Australia) was positioned at the beginning of ^{3}D$_{react}$ and ^{4}D$_{np}$, to trap and re-focus the H/C solutes from ^{2}D$_{IL}$ to ^{3}D$_{react}$ and/or trap and re-inject the oxime interconversion zones eluting from ^{3}D$_{react}$ to ^{4}D$_{np}$. A deactivated Press-Tight connector (Restek Corp) was used to connect the two columns. Isothermal operation (140 ˚C) was used for GC×GC experiments, whilst ^{3}D$_{react}$ and ^{4}D$_{np}$ were operated at various isothermal oven temperatures (140 – 160 ˚C). Helium was used as carrier gas (99.999% purity) with constant pressure (46 psi in ^{1}D$_{enant}$; 30.5 psi in ^{3}D$_{react}$). For stopped-flow analysis, the EPC for the DS was reduced to 2 psi (typically the lowest pressure setting that can be employed for the system, assumed to approximate stopped-flow experiments). The injector T was 230 ˚C, and injection volume 1 µL. Since QTOFMS was operated in total transfer of ion (TTI) mode through the quadrupole sector, this is referred to hereafter as accTOFMS. The ion source T, emission current and electron ionization voltage were set at 280 ˚C, 4.6 µA and 70 eV, respectively, with a mass range of 45–300 u. This system represents a 4D system, because the cryogenic modulation process mimics conventional GC×GC, the DS at the outlet of the second column operates as it would in MDGC, and a CT device at the inlet of the fourth column function to trap, refocus then reinject the resulting oxime distribution eluting from ^{3}D$_{react}$ to ^{4}D$_{np}$. 3D experiments (*e*GC-*D*GC-GC–accTOFMS, approximating a GC$_{enant}$ – GC$_{react}$ – GC$_{np}$ arrangement) were conducted using the same column configuration and conditions, but without GC×GC modulation.

Supporting Information (Section 1-2) provides further details of additional experimental methods (synthesis of 2-phenylpropanaldehyde oxime, GC-FID system, and data handling).

RESULTS AND DISCUSSION

Interconversion of 2-phenylpropanaldehyde oxime in *D*GC. The 1D chromatogram obtained using a polyethylene glycol (PEG) column demonstrated that 2-phenylpropanaldehyde oxime isomerizes on a time scale commensurate with the chromatographic separation process. Isomerization gives rise to a plateau between the terminal peaks of *E* and *Z* isomers, and at a higher T of 180 ˚C, only a single broad band is obtained, although much wider than an inert solute of the same retention (Supporting Information **Figure S2A**).

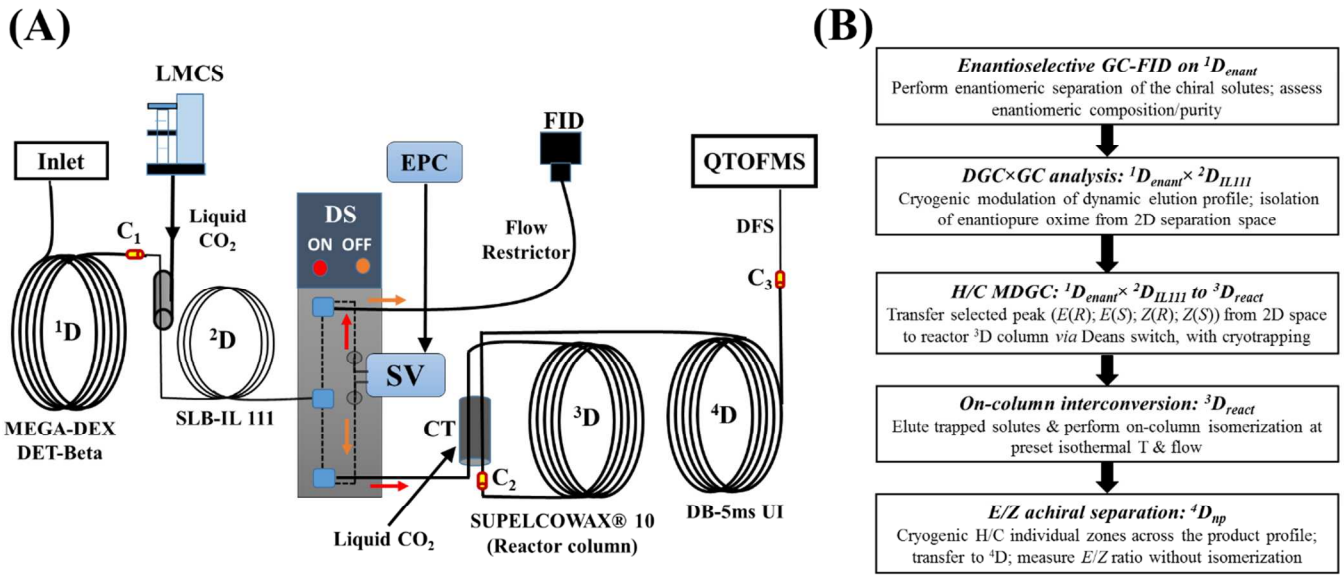

Figure 1. (A) Instrument schematic for *e*4D-*D*GC–accTOFMS. DS, Deans switch; ^{1}D: first, ^{2}D: second, ^{3}D: third, and ^{4}D: fourth dimension columns; DFS, deactivated fused-silica transfer line; CT, cryotrap; C_1 and C_2, press-fit union; C_3, capillary union; FID, flame ionization detector; LMCS, longitudinal modulation cryogenic system; EPC, electronic pressure control; SV, switching valve; QTOFMS, quadrupole-time-of-flight mass spectrometer. (B) Description of the process over the four column arrangement.

Separation of solutes into respective stereoisomers on the enantioselective column was observed without evidence characteristic of isomerism (Supporting Information **Figure S3**), indicating negligible interconversion. This is presumably because the chiral selector is dispersed in a low polarity methylpolysiloxane based matrix unlikely to promote interconversion;[36] it is assumed that interconversion of 2-phenylpropanaldehyde oxime proceeds primarily in the PEG stationary phase. As expected, an increase in T for the PEG phase increases the rate of reaction (i.e. faster *E*/*Z* isomerization), and eventually, the interconverting isomers appeared as a single broad peak (w_b ~ 39 s) without evidence of terminal peaks (Supporting Information **Figure S2B**).

An 'enantioselective+PEG' coupled-column ensemble with different lengths of the PEG phase was tested to obtain enantioseparation as well as to promote on-column isomerization. On the enantioselective column, the chiral oxime is both resolved into its (*E*)- and (*Z*)- isomers, with each isomer also enantioseparated into (*R*) and (*S*) antipodes. The PEG column then promotes interconversion of the two *E*/*Z* pairs of isomers (i.e. *R* and *S* enantiomers), which enter the PEG column at different times. This distribution envelope differs from the distribution when the isomers are directly injected into a single PEG column. If isomerization is slow compared to the chromatographic timescale (e.g. by using a relatively short PEG column) and the chiral stationary phase can distinguish between the enantiomers, four baseline-separated peaks will be obtained.

Figure 2A and **2B** illustrate the enantioresolution, interconversion region and retentions of *E*(*R*)-, *E*(*S*)-, *Z*(*R*)- and *Z*(*S*)-2-phenylpropanaldehyde oxime (note that the order of elution of the *R* and *S* enantiomers has not been elucidated). A shoulder marked with the arrow in Figure 2A preceding the *Z* isomers, will arise from interconversion of Z to *E* isomer as shown in Figure S2, and here is indicated to elute before the *Z* isomers on the PEG phase. At slower flow (Figure 2B) peak distortion becomes apparent due to increased isomerization. As interconversion kinetics increase (at higher T accompanied by reduced retention), the distribution of the isomers can collapse into a single, broad peak, which should progress into a narrower symmetric peak (i.e. $t_R(E) \sim t_R(Z)$) as the rate further increases.

In **Figure 2C** (w_b for first eluted peak > 60 s; w_b for second eluted peak > 80 s), both antipodes of the *Z* isomer were found to co-elute with the later *E* isomer when higher T is used, as verified by determination of their respective normalized peak area ratios. By using a longer PEG column (i.e. increased solute residence time, due to reduced flow), a larger proportion of the molecules undergo at least one interconversion event, with an elution profile characterized by a broad band (**Figure 2D**, band width > 10 min). This illustrates the inability of the separation process to adequately provide interpretation of the different overlapping species, with peak distortion indicative of extensive $E \rightleftharpoons Z$ isomerization. Note that using *D*GC×GC will assist in assigning all the relevant components in Figure 2 through physical separation of the total dynamic GC envelope. It is clear that on-column interconversions of several molecules at the same time can lead to quite complex peak profiles, with confounding competing reactions resulting in misinterpreted reaction kinetics. Based on these observations, *e*3D-*D*GC and *e*4D-*D*GC approaches were devised to investigate on-column *E*/*Z* isomerization reactions of 2-phenylpropanaldehyde oxime.

***e*3D-*D*GC–accTOFMS: ^{1}D Enantioselective–^{2}D PEG–^{3}D DB-5ms**. Initially, a three column strategy was evaluated, in which $^{1}D_{enant}$ separates the *E*/*Z* isomer maxima, and their corresponding enantiomers. Individual physically resolved *R*/*S* antipodes of the *E*/*Z* isomers in $^{1}D_{enant}$ can then be selectively H/C into $^{2}D_{react}$, to promote isomerization of the isomer at defined T and pressure. Thus it is not necessary to synthetically prepare individual pure *E* and *Z* isomers for separate study. PEG phases result in high interconversion rates for oxime molecules, so this was chosen as the reactor column. A liquid CO_2 static CT device was installed at the front section of the $^{2}D_{react}$ to retain H/C components after which the oven was cooled/heated to an appropriate T and/or pressure was reduced

to a preset setting, then closing the CO_2 supply to the CT releases them to elute under isothermal conditions.

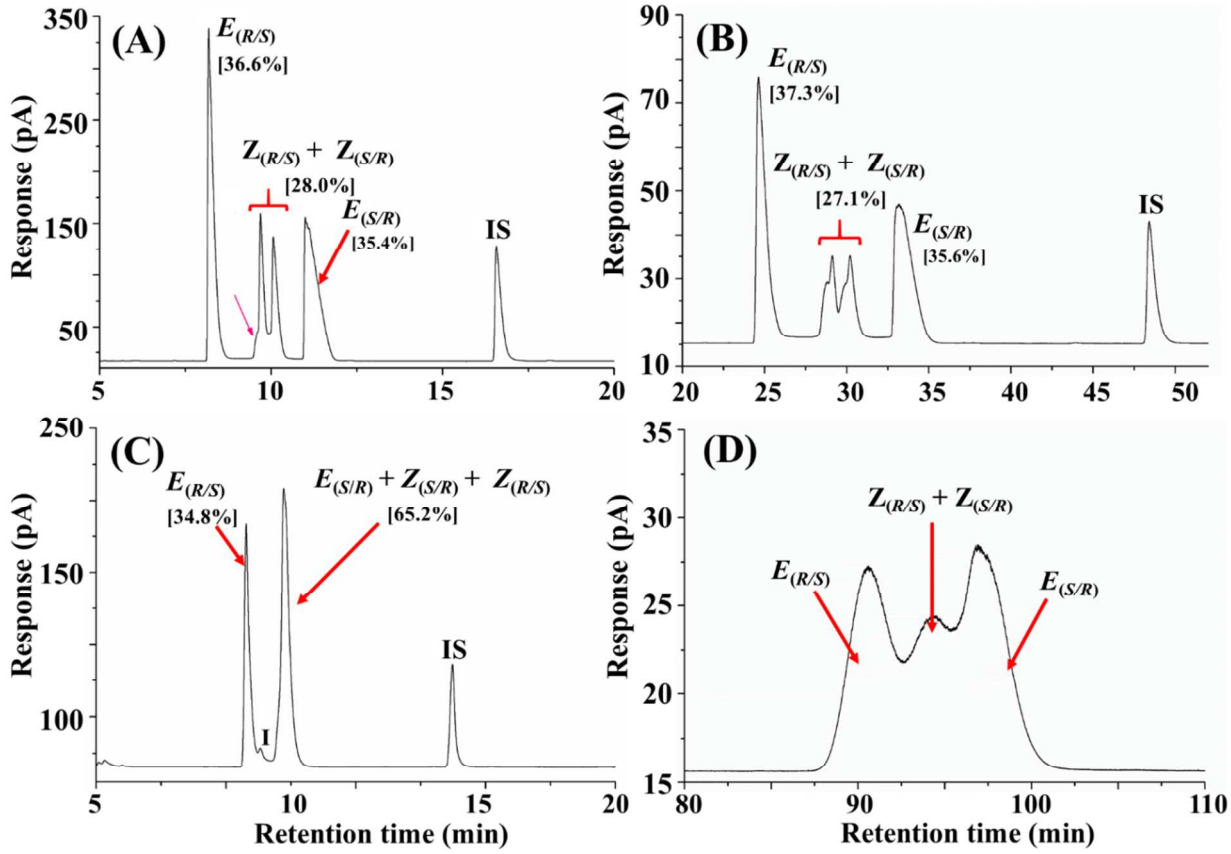

Figure 2. Chromatograms of 2-phenylpropanaldehyde oxime on an ensemble column pair (in enantioselective-PEG order) with PEG column lengths, oven T and column pressures of (A) 15 m, 130℃, 15 psi; (B) 15 m, 130℃, 5 psi; (C) 15 m, 150℃, 5 psi; and (D) 30 m, 130℃, 15 psi. IS, internal standard (1-tridecanol); I, impurity. Normalized peak area % were used to assist interpretation and peak assignments in (A), (B) and (C). Chromatographic interpretation of the interconversion region becomes difficult with an increased reaction rate.

An "on-the-fly" analysis of analyte peak shapes (e.g. based on a unified equation)[27] in which effluent is cryofocused at the static CT and directly remobilized to $^2D_{react}$ at the set oven T or pressure (with CO_2 supply to CT switched off and without a second dedicated oven and/or pressure program) is not appropriate for this study, because determination of rate constants depend on the employed pressure settings. Hence, the stopped-flow approach was applied here. Since rate constants depend on T, *e*GC–GC_{react} with cold trapping was evaluated for transfer of solutes, prior to oven cooling/heating and/or pressure change. Revolatilization of cryotrapped solute at the preset T allows isomer resolution into their corresponding *E*/*Z* isomers on $^3D_{np}$, and reduces the broadening or distortion of peak shapes arising from the $^2D_{react}$ column. System balance for H/C operation without leakage to the other channel is confirmed (Supporting Information **Figure S4**).

Figure 3A illustrates an example of a selected (asterisked) antipode corresponding to (*Z*)-2-phenylpropanaldehyde oxime successfully H/C, as shown in **Figure 3B**. On-the-fly analysis without cold trapping of the solutes eluting from $^2D_{react}$, results in a broad band (> 4 min) for the *E*-isomer which subsequently overlapped with the *Z* isomer (**Figure 3C**). A much better peak profile was obtained by applying cryogenic trapping then rapid delivery into the $^3D_{np}$ separation stage (**Figure 3D**), allowing precise determination of the isomeric ratio. It was observed that a small measure of interconversion of 2-phenylpropanaldehyde oxime occurred during enantiomeric separation in $^1D_{enant}$. Hence, direct H/C of the *E*/*Z* isomers in $^1D_{enant}$ might confound the correct determination of the interconversion isomeric ratios. For instance, DS operation of a specific region of $E_{(R/S)}$ isomer which contained an indeterminate amount of $Z_{(R/S)}$ isomer (i.e. the compound is not pure) to $^2D_{react}$ for isomerization processes, might result in incorrect estimation of the isomeric ratio, leading to erroneous rate constant values. Based on these observations, we devised an *e*4D-*D*GC approach to investigate on-column *E*/*Z* isomerization reactions of 2-phenylpropanaldehyde oxime, aiming to isolate and study all individual pure isomers. If interconversion does not proceed during enantiomeric separation, a modified *e*3D-*D*GC system can be employed, (Supporting Information **Figure S5**) in which the isomerized solute (together with corresponding interconversion plateau) eluting from $^2D_{react}$ can be cryotrapped at the inlet of $^3D_{np}$ via the cryogenically cooled trapping device and the trap rapidly moved upstream to allow isomer elution.

***e*4D-*D*GC–accTOFMS: ^{1}D Enantioselective×^{2}D IL 111–^{3}D PEG–^{4}D DB-5ms.** Integrating chemical reactions (here, interconversion) and multidimensional separations (GC×GC and H/C MDGC) in a single GC system relies on appropriate manipulation of solutes within the columns, possible switching of carrier flows, with precise control of pressure and DS balancing, and solute trapping and release as required. Of the five discrete steps described here (Figure 1B), $^1D_{enant}$ separates the *E*/*Z* isomers, and their corresponding enantiomers, according

to their retention factors with a small extent of *E*/*Z* interconversion. By proper choice of the ^{2}D column phase (here,

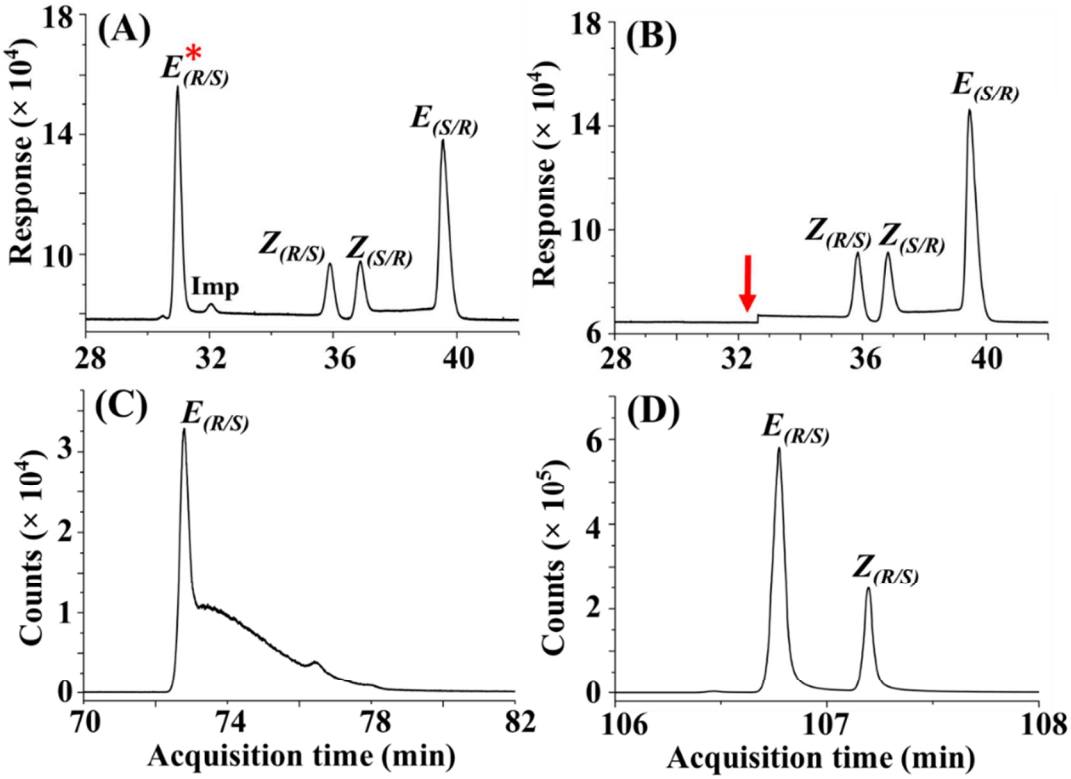

Figure 3. *e*3D-*D*GC–accTOFMS analysis of 2-phenylpropanaldehyde oxime: (A) $^{1}D_{enant}$ FID response; the peak to be H/C is asterisked; (B) $^{1}D_{enant}$ FID response, with (*R*/*S*)-*E* H/C to $^{2}D_{react}$; (C) Total ion chromatogram (TIC) of the H/C eluting from $^{3}D_{np}$ without cryogenic trapping at the inlet of $^{3}D_{np}$; (D) TIC of the H/C eluting from $^{3}D_{np}$ with cryogenic trapping at the inlet of $^{3}D_{np}$; Imp, impurity. The static CT is cooled to –25 ℃ and collects solute between 50 to 100 min, then the CO_2 supply was switched off to allow isomers to elute at about 6.8 min after release to $^{3}D_{np}$. Imp, impurity.

IL111 phase), it is possible to physically resolve (*E*/*Z*)-2-phenylpropanaldehyde oxime over the chromatographic profile. Individual resolved *R*/*S* antipodes of the *E*/*Z* isomers can then be selectively H/C from the 2D separation space into $^{3}D_{react}$, to promote isomerization of just that specific pure isomer at defined T and pressure. The selection of ^{2}D column phase (for GC×GC) requires careful consideration to balance the degree of resolution and interconversion in the ^{2}D fast column; a ^{2}D PEG and/or SLB-IL76 phase can promote rapid interconversion in ^{2}D (Supporting Information **Figure S6A** and **S6B**). This phenomenon can be visualized through a small increase in baseline (i.e. interconversion plateau) between the two resolved *E*/*Z* isomers on ^{2}D for a single modulation. A more substantial plateau will be found at higher T, accompanied by reduced resolution. Compromising between resolution, interconversion and good modulated peak shape (Supporting Information **Figure S7**), SLB-IL111 was chosen as the ^{2}D phase.

Without microfluidic DS transfer to $^{3}D_{react}$, isomers are displayed as classical contour or 3D plots typical of GC×GC. A liquid CO_2 static CT device was installed at the front section of the $^{3}D_{react}$ to retain components excised from the 2D separation space, after which the oven was cooled or heated to an appropriate T and/or with reduction of EPC pressure to approximate stopped-flow analysis; closing the CO_2 supply to the CT allows isothermal elution. Isomerized solute (and the interconversion plateau) eluting from $^{3}D_{react}$ is cryotrapped at the inlet of $^{4}D_{np}$ via the CT device. Revolatilization at the preset T allows isomer resolution into corresponding *E*/*Z* isomers on $^{4}D_{np}$, and reduces broadening/distortion of the peak shapes arising from the transfer of plateau zones from $^{3}D_{react}$. Both column head pressure and EPC pressure have to be finely tuned to obtain a balanced pressure setting for complete and quantitative flow diversion, particularly for vacuum detection. System balance for microfluidic switching without leakage to the other channel is confirmed (Supporting Information **Figure S8**).

Figure 4 illustrates an example of the operation of *e*4D-*D*GC–accTOFMS. Fast cryogenic modulation and GC separation at the end of $^{1}D_{enant}$, gives discrete separation on $^{2}D_{IL}$ of all the interconverting isomers (**Figure 4B**), as shown. Figure 4B represents the FID signal as the classical 3D plot typical of GC×GC operation. By applying DS sampling, a selected (asterisked) antipode corresponding to pure (*E*)-2-phenylpropanaldehyde oxime is H/C to $^{3}D_{react}$ in the next injection (**Figure 4C**). The targeted region (arrowed) has been excised from the 2D space (i.e. it is absent on the FID signal). Any band or region in the contour plot can thus be selected for diversion to $^{3}D_{react}$ depending on how the DS ON/OFF operation is chosen. On-the-fly analysis without cold trapping of the solutes eluting from $^{3}D_{react}$, results in a broad band (> 4 min) for the interconverted *E* isomer and overlapped with *Z* isomer (**Figure 4D**). A much better peak profile is obtained by cryogenic trapping then rapid delivery into the $^{4}D_{np}$ separation

stage (negating the effect of dispersion on $^3D_{react}$; **Figure 4E**), allowing for precise determination of the isomeric ratio, giving efficient trapping and transfer.

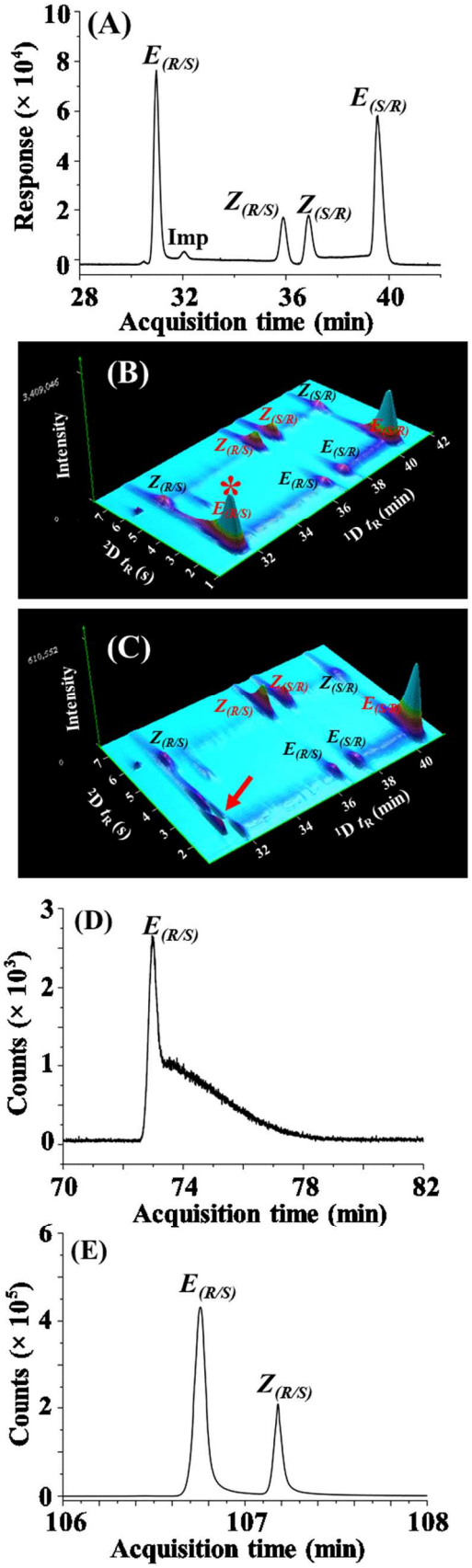

Figure 4. *e*4D-*D*GC–accTOFMS analysis of 2-phenylpropanaldehyde oxime: (A) $^1D_{enant}$ FID response; (B) 3D plot presentation without H/C, the peak to be H/C is asterisked; (C) microfluidic switching of (*R*/*S*)-*E*-oxime to $^3D_{react}$ removes this component from the 2D FID separation space; (D) TIC of the H/C $E_{(R/S)}$ component eluting from $^4D_{np}$ without cryogenic trapping at the inlet of $^4D_{np}$; (E) Equivalent result to (D) but now with cryogenic trapping at the inlet of $^4D_{np}$; the static CT is cooled to –25 ℃ and collects solute between 50 to 100 min, then the CO_2 supply was switched off to allow isomers to elute at about 6.8 min after release to $^4D_{np}$. Imp, impurity.

In the current set up, reaction T can be set independent of the separation T in $^1D_{enant}$×$^2D_{IL}$ and $^4D_{np}$, to control reaction rate, or time of reaction (via the column flow) in $^3D_{react}$. This can be interpreted as a high resolution strategy to employ a well-balanced microfluidic switching technique where one enantiopure isomer (consisting of multiple modulated peaks) is H/C from within the 2D separation space and transferred to $^3D_{react}$, which may be cooled/heated and/or with higher/lower pressure settings e.g. to adjust the interconversion kinetics. Then the isomerized fraction is separated in $^4D_{np}$ (*E*/*Z* peaks) to determine the *de novo* diastereoisomeric ratio for quantitative measurement of interconverting isomers that lead to the observed unresolved dynamic GC peak in 1D *D*GC. By repeat injection, this can be accomplished over the whole distribution, then conducted for different isothermal T or pressure settings.

Advantages of this design include: (i) it is unnecessary to isolate individual antipodes from a product mixture prior to GC analysis (i.e. analytes need not be pre-purified), since other components and impurities can be directly separated from solutes in $^1D_{enant}$×$^2D_{IL}$ and $^4D_{np}$ separation stages (Figure 4), which can be problematic for isomers which cannot be readily synthesized; (ii) a spot, band, or region of interest in the 2D space can be selected for diversion to the $^3D_{react}$; (iii) enrichment of enantiomers (i.e. of low abundance) can be achieved by multiple injections of the sample and directing target compounds into the cryogenically cooled static CT (at the inlet of $^3D_{react}$; Figure 1), to increase the mass of collected component.

This combines a number of contemporary GC methods (enantioselective GC, GC×GC, in-oven CT, on-column reaction GC, and H/C MDGC) into a single GC system to study interconversion of configurationally labile chiral molecules, or indeed any other like-processes, enabling separation and direct visualization of the species under study, and determination of rate constants. Mass-based deconvolution of the interconverting peak envelope here, e.g. by using accTOFMS, is usually not possible – the isomers often have the same mass spectra (Supporting Information **Figure S9**). A more selective MS dimension will enable extracted mass analysis ion product scans, for selective detection/analysis of molecules that undergo other transformations (for instance, thermally-induced transformations of terpenic molecules in essential oils[37-39]).

Reaction rate estimation. Both enantiomers of *E* (or *Z*) isomers have equal magnitude distribution coefficient (*K*) values in $^3D_{react}$ (achiral phase). When forward and reverse rate constants are equal ($k_f = k_b$), interconversion can be considered as a reversible first-order reaction.[40] The rate constants of isomerization (k) can then be calculated according to Eq S1 (**Section S3**, Supporting Information) from the experimentally obtained isomeric ratios of the major isomer just before elution (a_i) and

after elution (a_t) from the reactor column with the assumption that no isomerization takes place while the isomers were trapped during the brief oven heat/cool step. In several cases, the isomer ratios after interconversion (i.e. a_t) can be < 50% which are beyond the limit for calculation using Eq S1, e.g. resulting in a negative natural logarithm. With the assumption that $k_{E\rightarrow Z} = 0$ or $k_{Z\rightarrow E} = 0$, the pseudo-irreversible first order reaction can be applied.[40] k values can then be calculated according to Eq S2 (Section S3, Supporting Information).

In this study, it was observed that $k_{E\rightarrow Z} < k_{Z\rightarrow E}$ where $Z_{(R/S)} \rightarrow E_{(R/S)}$ yielding > 50% $E_{(R/S)}$. Thus, Eq S1 cannot be applied. However, it is also not effective to assume that $Z_{(R/S)} \rightarrow E_{(R/S)}$ is a pseudo-irreversible first order reaction since $E_{(R/S)} \rightarrow Z_{(R/S)}$ was also experimentally observed to be significant. This implies that Eq S2 cannot be effectively applied. Therefore, the calculation of k values obtained using both *e*3D-*D*GC–accTOFMS and *e*4D-*D*GC–accTOFMS experiments was performed, according to the direct solution of rate law for a reversible first-order reaction where only one species is present at the beginning of the reaction (a_i = 100%), as

$$\frac{a_t}{a_i} = \frac{k_b + k_f e^{-(k_f + k_b)t_{iso}}}{k_f + k_b} \qquad (1)$$

Eq S1 is the specific case of Eq 1 when $k_f = k_b = k$, and Eq S2 is derived when $k_b = 0$. Since there are two parameters (k_f and k_b) in Eq 1, at least two independent experiments are required. In this study, interconversion of individual (*E*, *R*/*S*)-, and (*Z*, *R*/*S*)-2-phenylpropanaldehyde oxime ($a_{i,E} = a_{i,Z}$ = 100%) was investigated and the calculation of rate constants can be obtained according to

$$\frac{a_{t,E}}{a_{i,E}} = \frac{k_{Z\rightarrow E} + k_{E\rightarrow Z} e^{-(k_{E\rightarrow Z} + k_{Z\rightarrow E})t_{iso}}}{k_{E\rightarrow Z} + k_{Z\rightarrow E}} \qquad (2)$$

$$\frac{a_{t,Z}}{a_{i,Z}} = \frac{k_{E\rightarrow Z} + k_{Z\rightarrow E} e^{-(k_{Z\rightarrow E} + k_{E\rightarrow Z})t_{iso}}}{k_{Z\rightarrow E} + k_{E\rightarrow Z}} \qquad (3)$$

$k_{E\rightarrow Z}$ and $k_{Z\rightarrow E}$ values can be obtained by fitting $a_{t,E}$ and $a_{t,Z}$ calculated by using Eq 2 and Eq 3 with the corresponding values obtained from the multidimensional experiments. Procedures for determination of t_{iso} are shown in **Section S4** (Supporting Information). Note that for stereoisomers that display different MS ionization probabilities (normally more pronounced in electrospray ionization), the isomeric peak areas have to be adjusted by appropriate correction factors. The calculated isomeric ratio, t_{iso}, and reaction rate constants of (*E*, *R*/*S*)-, and (*Z*, *R*/*S*)-2-phenylpropanaldehyde oxime for different pressure settings (including stopped-flow analysis) are summarized in **Table 1**. Isomeric ratios and rate constants derived using *e*3D-*D*GC and *e*4D-*D*GC show slight differences. However, in the case of complex samples where solutes suffer co-elution (particularly for plant derived extracts[37-39]) and/or isomerization at high temperature (i.e. leading to fast interconversion time), an *e*4D-*D*GC method will be necessary. For instance, **Figure 6** indicates elution profiles showing coalescence ($E_{(S/R)}$ overlaps both *Z* enantiomers) at elevated temperature (160 ℃), where chromatographic isolation of pure individual isomer is required to study its stereodynamics. The possible *E*/*Z* isomerization mechanisms of 2-phenylpropanaldehyde oxime may be proposed as nitrogen inversion, or rotation of the OH group around the C=N bond[41-43], as shown in **Figure S10** (Supporting Information). Whilst the exact mechanism remains uncertain, the reported kinetic data are still valid for the evaluation of *E*/*Z* isomerization of 2-phenylpropanaldehyde oxime on the PEG phase.

The precision of the *e*3D-*D*GC–accTOFMS and *e*4D-*D*GC–accTOFMS was assessed by repeating interconversion experiments five times on the same day (n = 5, intra-day precision), at 140 ˚C. The relative standard deviations (RSD) obtained for retention time in ^{1}D (< 0.20%), ^{2}D (< 2.27%), ^{3}D (< 0.10%) and ^{4}D (< 0.10%), and isomeric ratios (≤ 1.02%) are summarized in Supporting Information **Table S1**, demonstrating acceptable repeatability of the method. The first eluted isomer (*E* isomer) of each enantiomeric pairs is enriched during the chromatographic experiment (in 1D *D*GC with the PEG phases) because it is formed more rapidly than the first eluted isomer ($k_{-1} > k_1$), and the *Z* isomer is depleted to a greater extent due to its longer residence time in the reactor column.

Table 1. Forward and reverse rate constants measured by *e*3D-*D*GC–accTOFMS and *e*4D-*D*GC–accTOFMS methods (n=3).

Enantioselective multi-dimensional *D*GC	$E_{(R/S)} \rightarrow Z_{(R/S)}$			$Z_{(R/S)} \rightarrow E_{(R/S)}$		
	[a]Peak area *E* isomer (%)	t_{iso} (min)	$k_{E\rightarrow Z}$ ($\times 10^{-3}$ s^{-1})	[b]Peak area *Z* isomer (%)	t_{iso} (min)	$k_{Z\rightarrow E}$ ($\times 10^{-3}$ s^{-1})
*e*3D-*D*GC–accTOFMS	73.9 ± 0.1	29.6 ± 0.1	3.7 ± 0.8	29.2 ± 0.1	34.0 ± 0.1	10.4 ± 2.2
*e*3D-*D*GC$_{sf}$–accTOFMS	72.4 ± 0.2	37.2 ± 0.1	6.1 ± 1.0	27.6 ± 0.3	42.3 ± 0.1	15.9 ± 2.8
*e*4D-*D*GC –accTOFMS	72.5 ± 0.4	29.9 ± 0.1	3.1 ± 0.1	27.5 ± 0.4	33.2 ± 0.2	8.1 ± 0.2
*e*4D-*D*GC$_{sf}$–accTOFMS	73.6 ± 0.2	37.4 ± 0.1	4.6 ± 1.3	25.5 ± 0.2	42.2 ± 0.1	12.9 ± 3.6

[a] Peak area (%) of the *E* isomer peak, after isomerization. $E_{(R/S)}$ is H/C to ^{2}D$_{react}$ (*e*3D-*D*GC) or ^{3}D$_{react}$ (*e*4D-*D*GC) for interconversion.

[b] Peak area (%) of the *Z* isomer peak, after isomerization. $Z_{(R/S)}$ is H/C to ^{2}D$_{react}$ (*e*3D-*D*GC) or ^{3}D$_{react}$ (*e*4D-*D*GC) for interconversion.

sf correspond to stopped-flow experiments.

The described method should permit advanced chromatographic chemical isolation in 2D space, excising any target compound from the matrix, and permitting analysis of pure material under dynamic conditions. This approach does not specifically require a 'dynamic' reaction process to be studied, but is applicable to any situation requiring isolation and analysis. Potentially, this configuration also offers opportunities for investigation of interconversion processes of floral emissions such as scent profiles from Darwin's orchid and/or emissions from *Populus trichocarpa* trees containing a series of aldoxime species[38,39], allowing real-time online chromatographic sample extraction, where target components, resolved from matrix by the H/C process, are analyzed according to the above strategies to study dynamic behavior in real-time.

CONCLUSIONS

To the best of our knowledge, this is the first demonstration of a novel automated functional online *e*4D-*D*GC-MS system which incorporates a number of contemporary GC methods in the one integrated instrument, to study on-column isomerization reactions. The system provides initial assessment of enantiomeric composition of chiral molecules through $^{1}D_{enant}$ analysis with FID. GC_{enant}×GC_{IL} separation was performed in order to improve purity of solutes, then permitted interconversion of individual oximes to be studied. Microfluidic switching selects

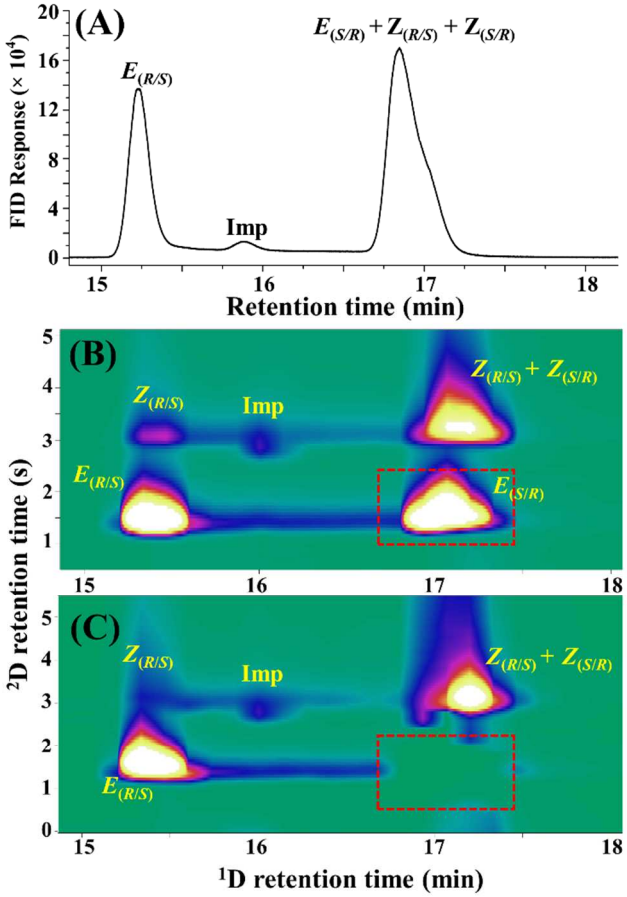

Figure 6. (A) $^{1}D_{enant}$ FID response; (B) 2D plot presentation without H/C with the peak to be H/C denoted by the dotted rectangle; (C) Microfluidic switching of compound *E*-2-phenylpropanaldehyde oxime from the end of $^{2}D_{IL}$ to $^{3}D_{react}$ removes the compound from the 2D separation space; the H/C component is absent on the FID signal whilst the remaining signal is almost identical to (B).

regions of the chromatographic elution from 2D space of a single pure stereoisomer for interconversion on $^{3}D_{react}$. Reacted products are quantified on $^{4}D_{np}$. This integrates a decision process based on pure component selection from either *e*GC (*e*3D-*D*GC) or *e*GC×GC (*e*4D-*D*GC) separation. Determination of *de novo* diastereoisomeric ratios by monitoring the whole time course of conversion of pure H/C isomers permits exact determination of isomeric ratios and calculation of rate constants. This is an advantage compared with usual 1D *D*GC methods, which require iterative comparison of experimental and simulated elution profiles to determine interconversion barriers. The described methodology could be applied to investigation of fast reactions (coalescing interconverting isomers) provided they take place on the chromatographic time scale. It should be a valuable adjunct for improved *D*GC methodology, offering high resolution and high throughput analysis as well as straightforward investigation of oxime molecular interconversion processes, which could be readily extended to investigation of stereodynamic interconversion or degradation processes of phytochemicals in plant extracts.[37-39]

ASSOCIATED CONTENT

Supporting Information

The Supporting Information is available free of charge on the ACS Publications website.

Additional details, calculation, and figures (PDF)

AUTHOR INFORMATION

Corresponding Author

*Email: philip.marriott@monash.edu

Notes

The authors declare no competing financial interests.

ACKNOWLEDGMENT

YFW gratefully acknowledges the provision of a Monash Graduate Scholarship and Monash International Postgraduate Research Scholarship. The authors would like to thank Assoc. Prof. Dr. David Lupton and Jacob Grant for synthesizing the 2-phenylpropanaldehyde oxime used in this study, and Dr. Sung-Tong Chin for technical assistance. We are grateful to MEGA s.n.c. for provision of the enantioselective column used in this project. PJM acknowledges the award of a Discovery Outstanding Researcher Award by the Australian Research Council, Grant DP1310217.

REFERENCES

(1) Akapo, S.; McCrea, C.; Gupta, J.; Roach, M.; Skinner, W. *J. Pharm. Biomed. Anal.* **2009**, *49*, 632-637.
(2) Shibukawa, M.; Miyake, A.; Eda, S.; Saito, S. *Anal. Chem.* **2015**, *87*, 9280-9287.
(3) Dugave, C.; Demange, L. *Chem. Rev.* **2003**, *103*, 2475-2532.
(4) Wolf, C. *Chem. Soc. Rev.* **2005**, *34*, 595-608.
(5) Scheer, A. M.; Mukarakate, C.; Robichaud, D. J.; Nimlos, M. R.; Carstensen, H. -H.; Ellison, G. B. *J. Chem. Phys.* **2012**, *136*, 044309.
(6) Welch, C. J.; Kress, M. H.; Beconi, M.; Mathre, D. J. *Chirality* **2003**, *15*, 143-147.
(7) Trapp, O. In *Differentiation of Enantiomers II*; Schurig, V., Ed.; Springer International Publishing: Cham, 2013; pp 231-269.
(8) Krupčík, J.; Mydlová, J.; Májek, P.; Šimon, P.; Armstrong, D. W. *J. Chromatogr. A* **2008**, *1186*, 144-160.
(9) Trapp, O.; Schurig, V. *J. Am. Chem. Soc.* **2000**, *122*, 1424-1430.
(10) Trapp, O.; Schurig, V. *Chem. Eur. J.* **2001**, *7*, 1495-1502.
(11) Trapp, O.; Trapp, G.; Schurig, V. *J. Biochem. Bioph. Meth.* **2002**, *54*, 301-313.
(12) Wolf, C.; Xu, H. *Tetrahedron Lett.* **2007**, *48*, 6886-6889.
(13) Maier, F.; Trapp, O. *Angew. Chem. Int. Ed.* **2012**, *51*, 2985-2988.
(14) Wistuba, D.; Trapp, O.; Gel-Moreto, N.; Galensa, R.; Schurig, V. *Anal. Chem.* **2006**, *78*, 3424-3433.
(15) Schoetz, G.; Trapp, O.; Schurig, V. *Anal. Chem.* **2000**, *72*, 2758-2764.
(16) Heegaard, N. H. H.; Jørgensen, T. J. D.; Cheng, L.; Schou, C.; Nissen, M. H.; Trapp, O. *Anal. Chem.* **2006**, *78*, 3667-3673.
(17) Liberek, B.; Augustyniak, J.; Ciarkowski, J.; Plucinska, K.; Stachowiak, K. *J. Chromatogr. A* **1974**, *95*, 223-228.
(18) Oswald, P.; Desmet, K.; Sandra, P.; Krupcik, J.; Armstrong, D. W. *Chirality* **2002**, *14*, 334-339.

(19) Wolf, C.; Pirkle, W. H.; Welch, C. J.; Hochmuth, D. H.; König, W. A.; Chee, G. -L.; Charlton, J. L. *J. Org. Chem.* **1997**, *62*, 5208-5210.
(20) Mazzanti, A.; Chiarucci, M.; Bentley, K. W.; Wolf, C. *J. Org. Chem.* **2014**, *79*, 3725-3730.
(21) Reich, S.; Trapp, O.; Schurig, V. *J. Chromatogr. A* **2000**, *892*, 487-498.
(22) Trapp, O.; Trapp, G.; Kong, J.; Hahn, U.; Vögtle, F.; Schurig, V. *Chem. Eur. J.* **2002**, *8*, 3629-3634.
(23) Schurig, V. *Chirality* **1998**, *10*, 140-146.
(24) Trapp, O.; Schurig, V. *Comput. Chem.* **2001**, *25*, 187-195.
(25) Trapp, O.; Shellie, R.; Marriott, P.; Schurig, V. *Anal. Chem.* **2003**, *75*, 4452-4461.
(26) Krupcík, J.; Oswald, P.; Spánik, I.; Májek, P.; Bajdichová, M.; Sandra, P.; Armstrong, D. W. *Analusis* **2000**, *28*, 859-863.
(27) Trapp, O. *Anal. Chem.* **2006**, *78*, 189-198.
(28) Trapp, O. *Chirality* **2006**, *18*, 489-497.
(29) Trapp, O. *J. Chromatogr. B* **2008**, *875*, 42-47.
(30) Bihlmeier, A.; Rotzler, J.; Rickhaus, M.; Mayor, M.; Klopper, W. *Phys. Chem. Chem. Phys.* **2015**, *17*, 11165-11173.
(31) Reich, S.; Schurig, V. *J. Micro. Sep.* **1999**, *11*, 475–479.
(32) Chifuntwe, C.; Zhu, F.; Huegel, H.; Marriott, P. J. *J. Chromatogr. A* **2010**, *1217*, 1114-1125.
(33) Marriott, P. J.; Trapp, O.; Shellie, R.; Schurig, V. *J. Chromatogr. A* **2001**, *919*, 115-126.
(34) Kröger, S.; Wong, Y. F.; Chin, S. -T.; Grant, J.; Lupton, D.; Marriott, P. J. *J. Chromatogr. A* **2015**, *1404*, 104-114.
(35) Mitrevski, B.; Marriott, P. J. *Anal. Chem.* **2012**, *84*, 4837-4843.
(36) Marriott, P. J.; Aryusuk, K.; Shellie, R.; Ryan, D.; Krisnangkura, K.; Schurig, V.; Trapp, O. *J. Chromatogr. A* **2004**, *1033*, 135-143.
(37) Filippi, J. -J.; Cocolo, N.; Meierhenrich, U. J. *J. Chromatogr. A* **2015**, *1383*, 134-143.
(38) Nielsen, L. J.; Møller, B. L. *Phytochemistry* **2015**, 120, 3-18.
(39) Irmisch, S.; McCormick, A. C; Boeckler, G. A.; Schmidt, A.; Reichelt, M.; Schneider, B.; Block, K.; Schnitzler, J. -P.; Gershenzon, J.; Unsicker, S. B.; Köllner, T. G. *Plant Cell* **2013**, *25*, 4737-4754.
(40) Krupčík, J.; Oswald, P.; Májek, P.; Sandra, P.; Armstrong, D. W. *J. Chromatogr. A* **2003**, *1000*, 779-800.
(41) Trapp, O.; Shellie, R.; Marriott, P.; Schurig, V. *Anal. Chem.* **2003**, *75*, 4452-4461.
(42) Andrzejewska, A.; Lapinski, L.; Reva, I.; Fausto, R. *Phys. Chem. Chem. Phys.* **2002**, *4*, 3289-3296.
(43) Nsikabaka, S.; Harb, W.; Ruiz-López, M. F. *J. Mol. Struc-THEOCHEM* **2006**, *764*, 161-166.

Table of Contents Graphic